The interactions of methyl tert-butyl ether on high silica zeolites: a combined experimental and computational study

UNIVERSITÀ DEGLI STUDI DI TORINO

The interactions of methyl tert-butyl ether on high silica zeolites: a combined experimental and computational study

V. Sacchetto,[ab] G. Gatti,[ab] G. Paul,[ab] I. Braschi,[bc] G. Berlier,[d] M. Cossi,[ab] L. Marchese,[ab] R. Bagatin[e] and C. Bisio*[abf]

[1]Department of Science and Technological Innovation and Interdisciplinary Nano-SiSTeMI Centre, University of Eastern Piedmont A. Avogadro, Viale T. Michel 11 – 15121 Alessandria, Italy;

[2]Department of Agricultural Science, University of Bologna, Bologna, Viale Fanin 44 – 40127 Bologna, Italy;

[3]Dipartimento di Chimica and NIS Centre of Excellence, Università di Torino, Via P. Giuria 7 -10125 Torino, Italy;

[4]Research Center for Non-Conventional Energy, Istituto Eni Donegani, Environmental Technologies, via Felice Maritano 26 - 20097 San Donato Milanese (MI), Italy;

[5]ISTM-CNR Istituto di Scienze e Tecnologie Molecolari, via G. Venezian 21, 20133 Milano, Italy;

Keywords: MTBE adsorption, fuel-based pollutants, high silica zeolites, FTIR spectroscopy, SSNMR, DFT ab initio calculations

Abstract

In this work, the interactions of methyl tert-butyl ether (MTBE) on different dealuminated high silica zeolites were studied by means of both experimental and computational approaches. Zeolites with different textural and surface features were selected as adsorbents and the effect of their physico-chemical properties (i.e. pore size architecture and type and amount of surface OH sites) on sorption capacity were studied. High silica mordenite (MOR) and Y zeolites (both with a SiO_2/Al_2O_3 ratio of 200) and ZSM-5 solid (SiO_2/Al_2O_3 ratio of 500) were selected as model sorbents. By combining FTIR and SS-NMR (both 1H and ^{13}C CPMAS NMR) spectroscopy it was possible to follow accurately the MTBE adsorption process on highly defective MOR characterized by a high concentration of surface SiOH groups. The adsorption process is found to occur in different steps and to involve isolated silanol sites, weakly interacting silanols, and the siloxane network of the zeolite, respectively. H-bonding and van der Waals interactions occurring between the mordenite surface and MTBE molecules were modeled by DFT calculations using a large cluster of the MOR structure where two adjacent side-pockets were fused in a large micropore to simulate a dealumination process leading to silanol groups. This is the locus where MTBE molecules are more strongly bound and stabilized. FTIR spectroscopy and gravimetric measurements allowed determination of the interaction strength and sorption capacities of all three zeolites. In the case of both Y and MOR zeolites, medium-weak H-bonding with isolated silanols (both on internal and external zeolite surfaces) and van der Waals interactions are responsible for MTBE adsorption, whereas ZSM-5, in which a negligible amount of surface silanol species is present, displays a much lower amount of adsorbed MTBE retained mainly through van der Waals interactions with zeolite siloxane network.

Introduction

The effective removal of fuel-based pollutants from waste waters is one of the most important and demanding environmental problem that have to be faced. Hydrocarbons and halogenated compounds are persistent organic pollutants mostly deriving from industrial waste and are especially present in waste water from oil refineries, petrochemical plants, and even from common petrol stations. Among all contaminants that can pollute waters, methyl tert-butyl ether (MTBE) deserves special attention in that it is the most common oxygenated fuel additive used to replace lead and increase the octane rating to promote complete burning of gasoline, thereby reducing CO and O_3 levels in urban air.[1,2]

MTBE is released to the atmosphere or ground water from a variety of sources including industrial discharges, spills and leakages of underground storage tanks or petroleum pipelines and mobile sources such as automobiles, during their refueling.[3] The small molecular size, the high solubility in water and low vapor pressure (ca. 43 mg L^1 and 249 mm Hg at 25 1C) combined with the near 100% solubility of MTBE in all gasoline components, may increase the total amount of this pollutant in ground water. MTBE toxicity is associated with its high mobility and persistency under both aerobic and anaerobic conditions in ground water. Although MTBE impacts on human health are not fully understood, it is already listed as a possible human carcinogenic agent.[2] Also, its low taste and odor threshold makes it undesirable for potable uses.[4]

For these reasons, the effective removal of MTBE from ground water is a problem of great importance and interest. Traditional methods normally used for pollutants removal such as air stripping, aerobic biodegradation and chemical oxidation reactions do not allow complete MTBE remediation from water. Physical adsorption has proven to be one of the most efficient methods for quickly lowering MTBE concentration in water.[5] In this respect, activated carbons, clay minerals, resins, and zeolites have been used as adsorbents for its removal from polluted water.[6] Conversely to what happens with activated carbons, the adsorption of MTBE into zeolites is not affected by dissolved organic matter always present in natural waters.[7] When the adsorption processes are carried out on microporous solids, many factors, such as pore volume, pore structure and size, composition, adsorption kinetics and temperature, initial pollutant concentration, could play an important role.[6] Furthermore, zeolites are stable over a wide range of conditions, including elevated temperature and acid environments and can be regenerated with removal of organic contaminants by heating treatment.

Several papers in the literature indicated that zeolites, especially those with distinct hydrophobic character (i.e. having high SiO_2/Al_2O_3 ratio) are capable to adsorb MTBE and other organic contaminants from water

at levels up to over an order of magnitude more efficiently than activated carbons.[8,9] Sorption results highlight the importance of pore size and SiO_2/Al_2O_3 ratio on contaminant removal,[9] and studies concerning the possible location of MTBE in channel systems of zeolites by means of thermogravimetric analysis and XRD studies were recently proposed.[10] In addition, experimental and computational studies related to the determination of diffusion properties of MTBE inside zeolite pores and to the understanding of the high MTBE sorption capacity of several zeolites can be found in the literature.[11]

Recently, a detailed study concerning the interactions of MTBE molecules with both external and internal surfaces of high silica Y zeolite was carried out by our research group.[12] This type of study was extended to other classes of high-silica zeolites, i.e. ZSM-5 and MOR, and the most relevant experimental and computational results are here presented. The zeolites were selected on the basis of their pore dimension, hydrophobicity, and structural defectivity, which was deeply investigated. The key-factors driving the adsorption processes of MTBE on high-silica ZSM-5 and MOR were identified and the obtained results were compared to those obtained on dealuminated Y zeolite by a combined FITR and solid state NMR study complemented with DFT calculations.

It is knowledge of the authors that MTBE displaces water molecules previously H-bonded to zeolite silanols (unpublished data) owing to its higher Lewis base character. This observation prompted the study of the adsorption of MTBE onto the dehydrated selected zeolites due to the intense infrared signals of water which mask spectral regions of interest for the elucidation of the zeolite–MTBE interactions.

Experimental methods

A. Materials

Methyl tert-butyl ether (MTBE) was purchased from Sigma-Aldrich with a purity of 99.9%. Highly dealuminated (high-silica) zeolite Y (hereafter named Y) powder in protonated form with a 200 SiO_2/Al_2O_3 molar ratio (code HSZ-390HUA) was purchased from Tosoh Corporation (Japan). Highly dealuminated zeolite ZSM-5 powder with a 500 SiO_2/Al_2O_3 molar ratio (code CBV28014) and highly dealuminated MOR zeolite powder in protonated form with a 200 SiO_2/Al_2O_3 molar ratio (code HSZ-690HOA) were both purchased from Zeolyst (USA).

B. Textural analysis

The specific surface area (SSA) of zeolites was measured by means of nitrogen adsorption at liquid nitrogen temperature (196 1C) in the pressure range of 7 10^6 to 1013 mbar (1 mbar = 100 Pa) using an Autosorb-1-MP (Quantachrome Instruments). Prior to adsorption, the samples were outgassed for 1 h at 90 1C, 1 h at 130 1C, and finally 16 h at 300 1C under high-vacuum conditions (final pressure = 1 10^9 mbar). The specific area of the samples was determined by the Brunauer– Emmett–Teller (BET) approach and using 0.01 p/p_0 as the value of maximum relative pressure. The pore size distribution was calculated by applying the cylindrical pore NLDFT method in the desorption branch.

C. Gravimetric analysis

MTBE adsorption isotherms were obtained at 35 1C on the Y, ZSM-5 and MOR samples outgassed for 2 h at 35 1C (MOR required an additional outgassing at 100 1C for 2 h to completely remove adsorbed water) by employing an Intelligent Gravimetric Analyzer (IGA-002, Hiden Analytical Ltd., U.K.), with integrated temperature and pressure controllers. The former consists of a thermostated water bath/circulator, employing a 50% water: 50% antifreeze (inhibited ethylene glycol) mixture. The latter is based on two pressure sensors, working in the 0–10 mbar (Baratron capacitance manometer, accuracy 0.05 mbar) and 10–1000 mbar (strain gauge, accuracy 1 mbar) ranges. IGA is an ultra-high-vacuum (UHV) microbalance (weighing resolution = 0.2 mg), specifically designed to study vapor sorption, which allows isotherms and the corresponding kinetics of adsorption and desorption to be determined. Buoyancy corrections were carried out using the weights and densities of all the components of the sample and counterweight sides of the balance and the measured temperature.

D. Thermogravimetric analysis

Thermogravimetry measurements were recorded with a SETSYS Evolution TGA-DTA/DSC thermobalance. Samples were heated from room temperature (rt) to 1100 1C at a heating rate of 5 1C min^{1} under oxygen (100 mL min^{1}).

E. FTIR spectroscopy

Infrared spectra were collected on a Thermo Electron Corporation FT Nicolet 5700 spectrometer with 4 cm^{1} resolution. Selfsupporting pellets of Y, ZSM-5 and MOR samples were obtained with a mechanical press at ca. 7 tons cm^{2} and placed into an IR cell equipped with KBr windows permanently attached to a vacuum line (residual pressure r 1 10^4 mbar), allowing all treatments and MTBE adsorption–desorption experiments to be carried out in situ. Spectra of MTBE adsorbed on zeolites have been collected at beam

temperature (ca. 35 1C) on samples previously dehydrated (under vacuum at beam temperature for Y and ZSM-5 zeolites and at 100 1C for MOR sample) or after outgassing 2 h at 500 1C.

F. Solid state NMR spectroscopy

All spectra were acquired on a Bruker Avance III 500 spectrometer and a wide bore 11.7 Tesla magnet with operational frequencies for ^{1}H and ^{13}C of 500.13 and 125.77 MHz, respectively. A 4 mm triple resonance probe with MAS was employed in all the experiments. The samples were packed on a Zirconia rotor and spun at a MAS rate between 10–15 kHz. The magnitude of radio frequency field was 100 kHz for ^{1}H MAS NMR and relaxation delays, d1, between accumulations was 5 s. For the $^{13}C\{^{1}H\}$ CPMAS experiments, the magnetic fields n^{H}_{rf} of 55 and 28 kHz were used for initial excitation and decoupling, respectively. During the CP period the ^{1}H RF field n^{H}_{rf} was ramped using 100 increments, whereas the ^{13}C C RF field n_{rf} was maintained at a constant level. During the acquisition, the protons are decoupled from the carbons by using a TPPM decoupling scheme. A moderate ramped RF field n^{H}_{rf} of 62 kHz was used for spin locking, while the carbon RF field n^{C}_{rf} was matched to obtain optimal signal and the CP contact time of 1 and 5 ms were used. All chemical shifts are reported using d scale and are externally referenced to TMS at 0 ppm.

MOR zeolite pre-treatment at 500 °C and MTBE adsorption were carried out directly on powder sample packed on the NMR rotor. For these purposes, the rotor was introduced in a special hand-made quartz cell that was connected to a high vacuum line (residual pressure p o 10^{4} mbar), allowing in situ heat treatment and adsorption processes. After zeolite outgassing at 500 1C for 2 h, MTBE in gas phase was adsorbed on the sample (at pressure of 0.5, 5, 10, and 20 mbar). In order to improve MTBE adsorption and diffusion through the powder, after contact with MTBE gas phase the rotor was frozen at liquid N_2 temperature for few minutes. Then it was extracted from the cell, rapidly closed and then sample was submitted to SS-NMR analysis (both ^{1}H and ^{13}C CPMAS NMR studies).

G. Models and ab initio calculations

Theoretical calculations have been performed with the TURBOMOLE6 package[13] at the DFT level with the B3LYP hybrid functional[14,15] and a basis set formed by the 6-31G(d)[16] atomic basis (a widely used Pople's double-z set plus polarization functions on heavy atoms) on oxygen and hydrogen atoms, and Hay and Wadt[17] effective core potentials (ECP) and basis set on silicon. After geometry optimization, the harmonic frequencies were computed at the same level.

To evaluate the van der Waals interactions, which can be very important in this kind of adduct and are known to be poorly reproduced by DFT methods, we used the empirical formulation proposed by Grimme[18]

and based on the classical atom–atom R-6 interaction approach, with atomic parameters fitted for different density functionals on the enthalpies of formation of a large set of organic molecules. Grimme's expression has been implemented with the parameters and the damping function described in ref. 18 using the scaling factor s6 = 1.05 as proposed for B3LYP.

As described below, a large cluster was extracted from the MOR zeolite periodic structure to model a segment of the main channel along with two side pockets, and a number of defects were added to simulate the formation of silanol groups due to the dealumination process. The procedure is illustrated in the ESI† (Fig. SM1–SM6).

Results and discussion

A. Material characterization

Three high silica zeolites with different physico-chemical properties are studied in this work. Y zeolite (FAU) is characterized by approximately 12 Å diameter cages, which are linked through access windows of 7.0 Å 7.1 Å in diameter and are composed of rings of 12 linked tetrahedra (12-membered rings, 12 MR).[19] Such a structure can also be viewed as formed by sodalite cages linked together through six-membered double rings to form the large cages mentioned above.

The framework type of the ZSM-5 zeolite can be described in terms of pentasil [5^4] units. The structure of ZSM-5 has a three dimensional pore system consisting of sinusoidal 10 MR channels (5.1 Å - 5.5 Å) and intersecting straight 10 MR channels (5.3 Å 5.6 Å). Because the 10 MR pore openings are lower than 12 MR, the shape selectivity for sorption distinctly differs from that of FAU.

Finally, the pore structure of MOR can be described as composed by four 5-MRs linked together forming chains. In fact, the topology of the framework is characterized by these chains connected to one another to form oval 12 and 8 MRs: the lining of the 12 MR channels contains 8 rings, but the 8 ring openings of adjacent 12 MR channels are displaced with respect to one another, so only very limited access from one channel to the next is possible.[20]

The different framework of the three zeolites allows quite large molecules to enter, especially in samples obtained after dealumination,[21,22] making these materials potentially useful in the adsorption of MTBE. N_2 adsorption at 77 K. Specific surface area and pore size distribution were determined by N_2 adsorption at 77 K in order to get some hints on the pore architecture of the three dealuminated zeolites (see Fig. SM7 in

ESI†). N_2 adsorption isotherms on all zeolite samples are of type I following IUPAC classification, thus indicating the presence of microporosities, as expected from the structural properties of zeolite samples. Nevertheless, especially in the case of ZSM-5 and Y samples, hysteresis loops of H3 type appeared in the 0.4–1 p/p_0 range, thus indicating the presence of mesopores that can be generated either by zeolite defectivity derived from dealumination processes or intraparticles aggregation (p/p_0 values higher than 0.8).

Textural properties of zeolites, derived from N_2 physisorption analysis, are reported in Table 1.

Table 1. Textural Properties of High-Silica Zeolites HSZ-Y, MOR, ZSM-5.

Sample	SSA_{BET}[a] (m^2g^{-1})	SSA_{microp}[b] (m^2g^{-1})	V_P[c] (cm^3g^{-1})	V_{microp}[b] (cm^3g^{-1})	V_{mesop}[d] (20-60 Å) (cm^3g^{-1})
Y	902	437	0.52	0.32	0.16
MOR	458	295	0.35	0.20	0.06
ZSM-5	533	283	0.39	0.16	0.14

[a]Brunauer–Emmet–Teller (BET) specific surface area (SSA). [b]Micropore surface area and volume by t-plot method. [c]Total pore volume by NLDFT method. [d]Volume of mesopores.

For zeolite Y, the specific surface area (SSA) is of 902 $m^2\,g^1$, half of which is due to the presence of micropores (437 $m^2\,g^1$) with a related volume of 0.32 $cm^3\,g^1$; ZSM-5 zeolite has a SSA of 533 $m^2\,g^1$, the presence of micropores is related by a SSA_{microp} of 283 $m^2\,g^1$ with a volume of 0.16 $cm^3\,g^1$. Finally, the MOR zeolite has a SSA of 458 $m^2\,g^1$, micropores have a SSA_{microp} of 295 $m^2\,g^1$ with a related volume of 0.20 $cm^3\,g^1$ (Table 1).

Two families of pores at ca. 13 and 22 Å are found on the Y zeolite (Fig. SM7B, ESI†). Micropores of ca. 8 Å are present in the ZSM-5 sample, along with mesopores whose diameter is in the 30–60 Å range. Finally, the MOR zeolite is characterized by the presence of three families of micropores of ca. 9, 11 and 14 Å, accompanied by a small fraction of intraparticle mesopores with a dimension between 25 and 70 Å. Although the micropore dimensions are overestimated for the use of nitrogen as probe molecule, the pore distribution gives a qualitative idea on how the dealumination process influences the overall pore volume and may lead to structural mesoporosity. It is known, in fact, that the dealumination process modifies the zeolite pore architecture, enlarging the windows between interconnected cages with the formation of mesopores or large micropores.[23] This process leads also to the production of a significant concentration of internal silanols (vide infra).

Infrared spectroscopy. Surface properties of dealuminated zeolites were studied by IR spectroscopy upon water removal (Fig. 1). The IR spectrum of dehydrated MOR zeolite (Fig. 1A, a) is characterized by the presence of a band at 3730 cm^{1}, and of a broad absorption extending in the region between 3700 and 3200 cm^{1}. More specifically, the large absorption is composed by at least two components, one at around 3670 cm^{1} and another one with a maximum at ca. 3460 cm^{1}. A band at 3730 cm^{1} was already observed in dealuminated MOR zeolites and was assigned to hydroxyl groups formed at places left vacant by aluminum atoms.[24] Moreover, a band at 3670 cm^{1} was also observed and assigned to OH groups formed at the places left by the more easily removable framework aluminum atoms.[24] Olsson and Rollman[25] suggest that such atoms would be located at T2 sites where the lowest T–O bond (1.607 Å, T being Al or Si) compared with the other locations favors a preferential aluminum removal. Finally, the large and intense band in the 3600–3200 cm^{1} range is due to Si–OH groups interacting each other through H-bonds and its presence strongly suggests that the MOR sample is characterized by a high surface defectivity.[26,27]

H-bonded SiOH groups are also present in Y zeolite but in a lower amount with respect to MOR zeolite. In addition, the IR spectrum of the Y (Fig. 1A, b) presents absorptions at 3745 and 3740 cm^{1}, corresponding to the vibration of OH groups located on the external and internal (i.e. inside the zeolite cage) surface of the Y crystals, respectively.[12]

Different characteristics are present in the IR spectrum of dehydrated ZSM-5 zeolite (Fig. 1A, c). This sample does not contain clearly detectable isolated silanols and only a broad and weak band is present in the 3600–3000 cm^{1} range, thus attesting the presence of a small concentration of silanol groups mainly interacting through H-bonding.

The intensity of bands related to OH species on the surface of the three zeolites merits some additional observations: the surface of the MOR sample is heavily dominated by H-bonded silanol groups, whereas a large fraction of isolated SiOH groups are present in the cages of the Y sample.

All dealuminated zeolites were outgassed up to 500 1C to cause the condensation of H-bonded silanol species, thus reducing both the heterogeneity of the surface OH sites and the complexity/ intensity of the absorptions at 3700–3000 cm1 (Fig. 1B). Upon outgassing the MOR sample at high temperature (Fig. 1B, a) the population of SiOH groups interacting with each other through H-bonding (broad absorption in the 3600–3200 cm1) is strongly reduced. Indeed, upon heating main bands at 3745 and 3735 cm1 are found in Y and MOR samples, with additional absorptions at ca. 3650 and 3500 cm1 in the MOR spectrum.

Thermogravimetric analysis. To describe quantitatively the content of silanol groups of MOR and Y

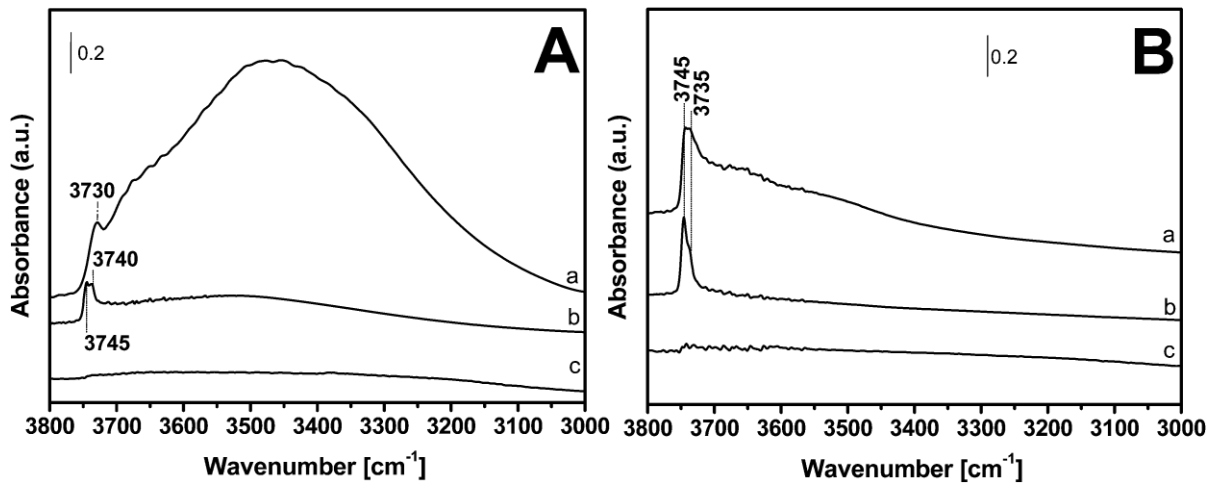

Fig. 1 FTIR spectra of high-silica zeolites MOR (a), Y (b), and ZSM5 (c) after outgassing at low temperature (i.e. rt for both Y and ZSM5 and 100 1C for MOR) (A) and after outgassing at 500 1C the same samples (B).

zeolites, thermogravimetric analysis was performed (Fig. SM8, ESI†). The amount of silanols was determined considering the weight loss within the range of 150–1000 1C, whereas adsorbed water is released from the pores in the temperature range from rt to 150 1C. The Y sample contains a lower amount of water (ca. 2 wt%) with respect to MOR (ca. 7 wt%). From 150 1C to about 1000 1C, the zeolite frameworks are progressively dehydroxylated. The weight loss in this temperature range, which differs among the two zeolite structures, can be attributed to water released from silanol condensation. The amount of silanol groups can therefore be estimated by the weight loss between 150 and 1000 1C. This amount is

approximately 0.8 wt% and 2.3 wt%, corresponding to 0.56 and 3.71 OH per nm2, for Y and MOR zeolites respectively.

The high concentration of silanols of the MOR sample, in good agreement with the intensity of the IR bands (Fig. 1), explains the ability of this sample to adsorb relevant amount of water, which is likely stabilized in the side pockets where the defects are mainly located (Fig. SM6, ESI†). It has to be underlined that adsorbed water is fully removed from the MOR sample only after outgassing at 100 1C, whereas on Y and ZSM-5 a treatment at rt is sufficient.

Finally, the TG analysis allowed the concentration of silanols to be quantified upon outgassing at increasing temperature. The case of the MOR sample is here relevant for the implication in the MTBE adsorption, which will be discussed in the following section. Considering the weight losses at 150 and 500 1C the sample shows per unit cell (u.c.) ca. 7 OH per u.c. (2.3 wt%) and 4 OH per u.c. (1.4 wt%), respectively.

Models and ab initio calculations. Computational studies were carried out to obtain some hints on the different types of SiOH species produced by the dealumination process in the high silica MOR zeolite. Vacancies due to the aluminum removal tend to migrate and reduce somewhat the number of silanols, creating islands of nested Si–OH groups: it has been observed that such structural modifications can lead to the enlargement of the side-pockets,28 and this feature is likely to play an important role in the adsorption of different molecules, like MTBE.

To model the MTBE–MOR system a rather large cluster was defined, with stoichiometry $Si_{84}O_{124}H_{82}(OH)_6$, featuring a segment of the main channel approximately 14 Å long with a lateral cavity obtained from the fusion of two side-pockets (as a result of the dealumination process). Such a cluster contains six silanol groups, and 82 additional hydrogen atoms used to saturate the external Si valencies: the procedure followed to build this model is described in greater detail in the ESI.† This cluster roughly corresponds to one and a half unit cell along the direction of the main channel, so that the concentration of silanol groups is consistent with the unit cell stoichiometry of the sample treated at 500 1C (ca. 4 OH per u.c.) defined above on the basis of TGA analysis.

The geometry of the model cluster was optimized at the DFT level, with the functional and basis sets indicated above, with the result illustrated in Fig. 2. The harmonic vibrational frequencies for the silanol stretching modes were computed at the same level and they are listed in Table 2, second column (to reduce the computational burden, the frequencies were obtained with a numerical differentiation of gradients, with respect to the coordinates of 18 atoms only, i.e. the six Si–O–H groups of interest).

It is useful to compare the Si–OH stretching frequencies with the frequency calculated at the same level for an isolated silanol (Fig. 2(d)), since this shift is a measure of the perturbation due to the interactions with the zeolite walls or the surrounding silanols, and it can be compared to the analogous experimental data with less systematic errors. The computed frequencies for the model silanols range from 3766 to 3610 cm^{1}, with shifts with respect to the isolated silanol of few tens to almost 200 cm^{1}. The smallest shift (i.e. the highest frequency) is computed for a silanol accepting an H-bond from a nearby partner, which in turn exhibits the largest shift (196 cm^{1}, a clue of a rather weak H-bond, as confirmed by the quite long O–O distance, 2.84 Å); the shifts computed for the other silanols indicate varying (generally weak) interactions with each other and with the silicate structure.

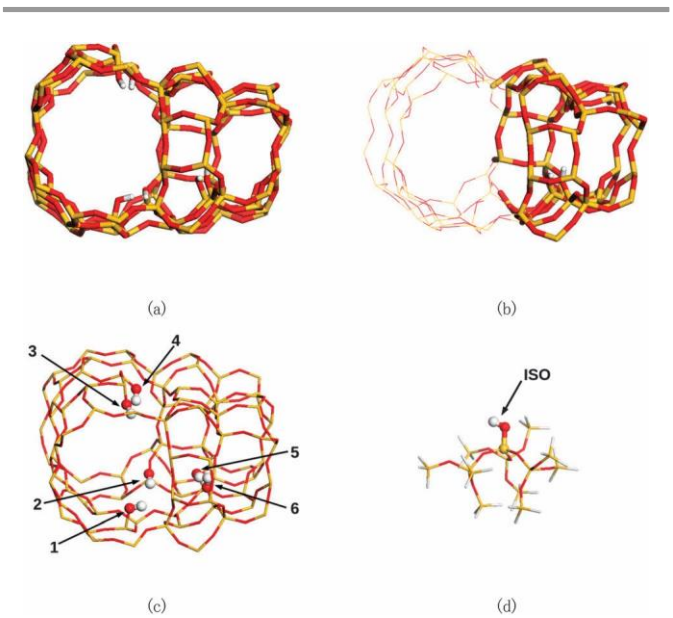

Fig. 2 Model cluster used to simulate the MOR internal silanols: (a) view along the main channel direction; (b) the lateral cavity obtained by fusing two adjacent side-pockets; (c) the six silanol groups present inside the cluster; (d) for reference, a model of an isolated silanol, used in ref. 12 to describe the groups on the zeolite external surface, presenting the highest vibrational frequency. In the cluster pictures (a–c) the external H atoms added to saturate the Si valencies are not shown.

Table 2. Harmonic frequencies (cm^{-1}) computed at the DFT level for the OH stretching vibration of silanol models of Figure 3; for comparison, the stretching frequency of on isolated silanol computed at the same level is also reported. In parentheses the frequency shifts after MTBE adsorption with respect to the bare cluster silanols.

Silanol (Figure 3)	Cluster	Cluster + MTBE (I)	Cluster + MTBE (II)	Cluster + MTBE (III)
ISO[a]	3806			
1	3695	3195 [b] (-500)	3712 (+17)	3497 [b] (-198)
2	3683	3686 (+3)	3690 (+7)	3672 (-11)
3	3645	3625 (-20)	3701 (+56)	3677 (+32)
4	3618	3598 (-20)	3658 (+40)	3630 (+12)
5	3610	3585 (-25)	3034 [b] (-576)	3191 [b] (-419)
6	3766	3771 (+5)	3436 (-330)	3467 (-299)

(a) ref. 12.
(b) H-bonded to MTBE.

This cluster is only one of the many possible models of the internal structure of dealuminated MOR zeolite: nonetheless it contains some important features, which are likely to influence the host–guest interactions, in particular the fusion between adjacent side pockets, predicted by Monte Carlo calculations and confirmed by microscopic observations.[28]

The calculated frequencies are approximated due to anharmonicity effects and to the quite limited basis set adopted, due to the large size of this model. However, the computed shifts agree well with the IR spectra (Fig. 2(b)), showing a combination of broad bands shifted by 40–200 cm^1 with respect to the sharp absorption attributed to external isolated silanols (recorded at 3745 cm^1).

B. Monitoring the interaction of MTBE with MOR zeolite

IR spectroscopy was used to study the interactions between increasing doses of MTBE in the vapor phase and surface adsorption sites of the different high silica zeolites.

Since ZSM-5 zeolite does not show a significant concentration of silanol species and studies of MTBE adsorbed on zeolite Y were already reported,[12] only the complete MTBE adsorption experiment on MOR zeolite is here described (Fig. 3). To understand better the interactions occurring between the surface sites of MTBE on MOR zeolites, the OH concentration of this high silica zeolite was reduced by pretreating the material at 500 1C.

The admission of the highest MTBE dosage (100 mbar) (Fig. 3,b) led to the disappearance of SiOH groups originally absorbing at 3745, 3735 and ca. 3650 cm^{1}, that appear as negative bands in the difference spectrum (see also inset on the left side of Fig. 3). The negative band at 3745 cm^{1}, narrow and intense, is asymmetric with a tail that strongly overlaps the weaker and broad band at 3650 cm^{1} envisaging the presence of silanols originally absorbing at ca. 3720–3670 cm^{1}. As a consequence of MTBE adsorption, a broad band in the 3700–3000 cm^{1} range with two strongly overlapped components at ca. 3220 and 3340 cm^{1} is formed. This broad band originates from the interaction of silanol groups with MTBE oxygen atom through H-bonds[12] (Scheme 1).

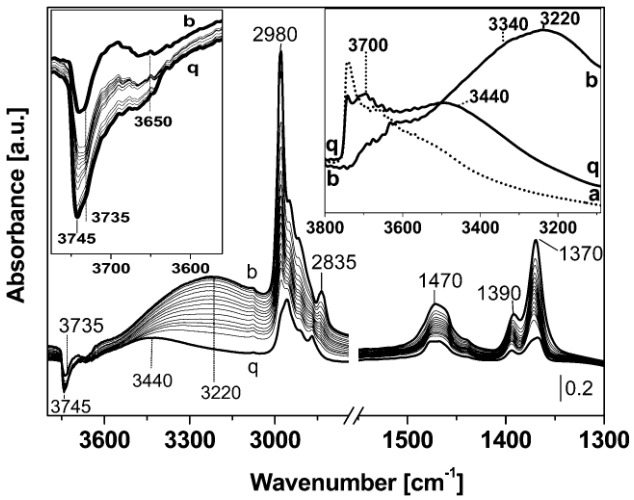

Fig. 3 Difference infrared spectra of increasing doses of MTBE (P_{max} = 100 mbar) on high-silica MOR zeolite outgassed at 500 1C. The spectrum of the bare sample after heating treatment (inset, curve a) was used as a reference and subtracted from all spectra obtained after exposure to MTBE vapor. In the inset on the right side, absorption spectra collected before (a) and after (b) adsorption of high MTBE doses, and its prolonged outgassing (q) at rt are reported. The inset on the left side reports an enlarged view of difference spectra of MTBE absorbed on zeolites in the 3800–3525 cm^{1} range.

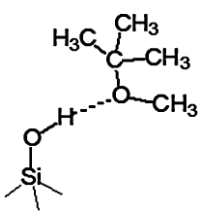

Scheme 1 Qualitative representation of H-bonding between surface silanols and MTBE molecule.

Stretching and bending vibrations of the methyl groups of MTBE molecules are found in the 3000–2800 and 1500–1300 cm^{1} spectral regions, respectively. In particular, the IR spectrum of adsorbed MTBE presents bands at 2980, 2915, 1390, and 1370 cm^{1} that are related to CH_3 stretching and bending vibrations, respectively, of the tert-butyl group whereas those at 2950 and 2835 cm^{1} are due to the CH_3 symmetric stretching of the methoxyl group.[12]

By decreasing the MTBE dosage from 100 to ca. 10 mbar (spectra b–f in Fig. 3), bands due to CH_3 stretching and bending modes decrease in intensity, whereas absorptions due to the formation of H-bonds between the ether and the surface silanols remains unaltered. As determined by microgravimetry (vide infra) at 10 mbar the concentration of adsorbed ether is ca. 7 MTBE per u.c.: many molecules would not fit easily inside the pores (as suggested also by the simulated MTBE/MOR adducts discussed below), so that part of the MTBE is likely adsorbed on the external surface. In such external layers, MTBE molecules are expected to be in a liquid-like state, whereas inside the zeolite the ether is involved in van der Waals interactions with the silica framework.

As a matter of fact, spectra of MTBE adsorbed at high pressure on MOR zeolite also display features typical of the molecule in a liquid-like phase (see Fig. SM10 in ESI†), as already observed for MTBE adsorption in Y zeolite.[12]

At pressure below 2 mbar (Fig. 3, curve g), the bands due to MOR silanol groups interacting with MTBE start to decrease in intensity, and a progressive decrease of absorptions related to stretching and bending vibration of CH_3 groups is also observed. In this pressure regime the main band at 3220 cm^{1} due to silanols interacting with ether molecules decreases in intensity upon reduction of the MTBE doses, and different components at higher frequencies (at ca. 3340 and 3440 cm^{1}) become more evident. In parallel, the band at 3745 cm^{1} is less negative and the components at 3735 and 3650 cm^{1} progressively become more pronounced (see inset on the left side of Fig. 3).

This experiment clearly shows that the band at 3745 cm^{1} is restored in correlation with the decrease of the band at 3220 cm^{1}, suggesting that the strongest H-bonds established between MTBE and isolated silanol species located on the MOR external surface of MOR crystals: for these silanols, the wavenumber shift ($\Delta\nu_{OH}$) due to MTBE adsorption is ca. 500 cm^{1}.

The band at 3340 cm^{1}, assigned to the internal silanols originally absorbing either at 3735 or at 3720–3670 cm^{1} and now bonded to MTBE, appeared more stable during the outgassing procedure, even if these H-bonds are weaker than the bonds formed to external silanols (as indicated by the smaller $\Delta\nu_{OH}$, ca. 400 cm^{1}

in this case). Moreover, a fraction of MTBE remains irreversibly adsorbed in the zeolite giving absorptions at ca. 3440 and 3700 cm^{1} (Fig. 3, right inset), associated with the negative bands at 3735 and 3650 cm^{1} (Fig. 3, left inset). This association indicates that the residual MTBE molecules are H-bonded either to isolated internal silanols (originally vibrating at 3735 cm^{1}) or to silanol couples or groups, weakly interacting with each other (originally vibrating at 3650 cm^{1}).

The persistency of irreversibly adsorbed MTBE, even if involved in weak H-bonds with internal SiOH species, shows that confinement effects play an important role in stabilizing the ether molecules inside the zeolite cages through dispersive forces, in agreement with computational studies (vide infra). This type of behavior was also observed for zeolite Y.[12] Besides 1:1 silanol–ether adducts, the formation of multiple H-bonds of ether with SiOH species cannot be excluded in the restricted space of MOR side pockets (see structure III of Fig. 4).

To simulate the silanol stretching frequencies after adsorption, one MTBE molecule was inserted in the model cluster described above and the adduct structure was optimized starting from different geometries. Three distinct minima were found, corresponding to the structures illustrated in Fig. 4: in conformations I and II MTBE is H-bonded to a single silanol group, while in III two H-bonds are established. The O–O distances in these H-bonds are 2.66 Å (structure I), 2.63 Å (II), 2.69 and 2.80 Å (III): then, likely due to the different mobility of MTBE in the various parts of the cluster and to the interactions with the rest of the zeolite walls, the strongest H-bond is formed in structure II (such a short O–O distance is actually typical of a strong bond), while in structure III both H-bonds are weaker, as a result of the compromise between various interactions.

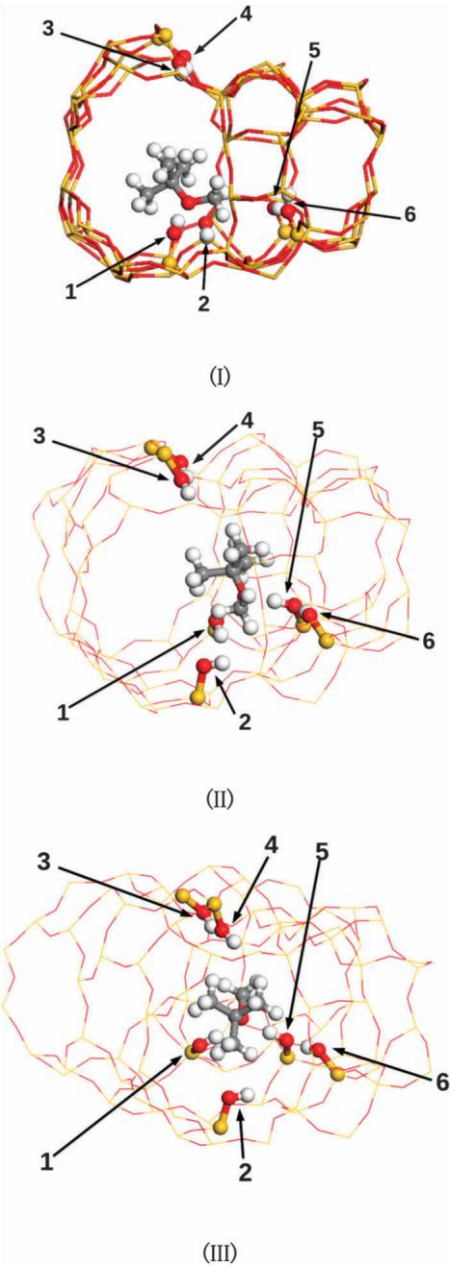

Fig. 4 MTBE–MOR cluster adducts optimized at the DFT level in different conformations: (I) and (II) MTBE H-bonded to one cluster silanol; (III) MTBE H-bonded to two cluster silanols.

The main contributions to MTBE–MOR binding energy come from H-bonding to silanols and from dispersion (van der Waals) interactions with the overall zeolite structures: the adducts of the same molecule with Y zeolite was already studied in ref. 12, finding a comparable strength for H-bond and van der Waals energies. Following the same approach as in the aforementioned paper, dispersion interactions were

estimated with Grimme's empirical formula and parameters applied to the geometries optimized at the DFT level: the H-bond (E_H) and van der Waals (E_{vdW}) energies were defined as

$$E_H = E_{DFT}(\text{MTBE–cluster}) - E_{DFT}(\text{cluster}) - E_{DFT}(\text{MTBE})$$

$$E_{vdW} = E_{DFT\text{-}disp}(\text{MTBE–cluster}) - E_{DFT\text{-}disp}(\text{cluster}) - E_{DFT\text{-}disp}(\text{MTBE}) - E_H$$

where $E_{DFT\text{-}disp}$ indicates the sum of B3LYP and Grimme's dispersion energy; the binding energies are listed in Table 3. These results can be compared with the energies computed for MTBE in Y zeolite,[12] E_H being generally smaller and E_{vdW} slightly higher: actually, MOR pores and channels are narrower than Y cages, which can cause a larger steric hindrance (thus less effective H-bonding) and greater interactions with the zeolite walls.

The corresponding stretching frequencies are listed in Table 2, columns 3 to 5 (also in this case the frequencies have been obtained by numerical differentiation of gradients, considering only the six silanol groups). As expected, the vibrational frequencies of Si–OH involved in the H-bonds with the ether are strongly shifted to smaller wavenumbers, in good correlation with the O–O distances reported above. In addition, the presence of MTBE perturbs the geometry and polarizes somewhat also the other silanols, so that the shifts are slightly modified with respect to the isolated model cluster; in structures II and III we note that a stronger internal H-bond is formed between silanol groups 6 and 5 (Fig. 4) with corresponding shifts of the stretching frequency of 370 and 339 cm^1, respectively.

The computed frequencies and binding energies agree satisfactorily with the proposed interpretation of IR spectra: after MTBE addition, absorption bands at low wavenumbers appear, shifted with respect to external isolated silanols by 300–400 cm^1, in good agreement with structures I and III predicted by the calculations (the wavenumber shift of 576 cm^1 determined for structure II is somewhat too large if compared with experimental results). Since the interaction energy is a sum of two quite large and comparable contributions, due to H-bonding and van der Waals interactions, we can rationalize the behaviour observed during MTBE desorption, when the IR bands at the lowest wavenumbers (thus associated with the strongest H-bonds) vanish faster than other bands at higher wavenumbers. It is apparent that the latter bands are due to adducts with a larger overall interaction energy, though the H-bond contribution is not the largest possible.

Interactions occurring between MTBE and MOR zeolite were also studied by means of ^1H and ^{13}C MAS-NMR spectroscopy. ^1H MAS NMR provides direct information about the different proton sites present in the zeolite system. The proton spectrum of the MOR sample previously treated at 500 1C recorded at room

temperature with a MAS rate of 15 kHz (Fig. 5(a)) shows a main signal at 1.7 ppm, attributed to isolated silanols.[29] A broad peak appearing as a shoulder to the intense peak in the range 2–3 ppm is due to silanol species interacting each other via hydrogen bonding. The presence of these SiOH species on the surface of MOR zeolite was already pointed out by FTIR spectroscopy (vide supra). Furthermore, the proton signal at 3.9 ppm is due to residual Brønsted acid sites (Si(OH)Al species)[30] which are still present in the dealuminated MOR zeolite, even though in much lower concentration than silanols.

On the other hand, the ^{1}H MAS NMR spectra of MTBE adsorbed on the MOR sample (Fig. 5(b)–(e)) show resonances due to t-butyl methyl as well as methoxy protons. At very low pressure (0.5 mbar), the spectrum is dominated by sharp signals from MTBE in the adsorbed state (t-butyl methyl protons at 0.9 and methoxy protons at 3.5 ppm) as seen in Fig. 5(b). However, at higher pressures (5, 10 and 20 mbar) additional signals from MTBE in the condensed state (i.e. mutually interacting with other MTBE molecules and weakly interacting with the zeolite framework) appeared as well (t-butyl methyl protons at 1.1 ppm and methoxy protons at 3.1 ppm). Moreover, the chemical shifts of these narrow signals for t-butyl methyl protons and methoxy protons are closely matched with the shifts observed in the liquid state (spectrum not shown) for MTBE. In addition, signals from MTBE adsorbed on the MOR surface appeared as broad signals beneath the sharp ones. What is more striking is the appearance of a broad resonance centered at 6.4 ppm as well as a signal at 4.6 ppm after MTBE adsorption. These features account for the formation of H-bonding interactions between the MOR silanol groups and MTBE. The appearance of such resonance peaks are in agreement with FTIR data (vide supra), from which the formation of mediumweak H-bonding between the SiOH surface species and MTBE molecules is well observable (Dn_{OH} after MTBE interaction being of 400–500 cm^{1}, depending on the location of silanols on the zeolite surface). MTBE molecules undergo different binding dynamics and form spatially structured clusters of variable sizes with chemical shift values determined by exchange between bound MTBE, free MTBE, isolated SiOH, hydrogen bonded SiOH and bridging OH protons. Of these, hydrogen bonded silanols resonate around the broad peak centered at 6.4 ppm. The breadth of this signal spanning from 3 to 9 ppm can be ascribed to heterogeneous broadening associated with an extensive distribution of chemical shifts provided by a wide distribution of H-bonds. It is important to note that several types of MTBE H-bonded to silanols are found by FTIR and these species can give broad NMR resonances.

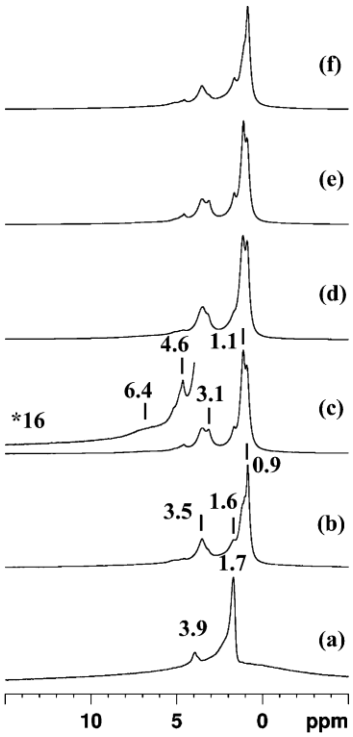

Fig. 5 ^{1}H MAS NMR spectra of zeolite MOR treated at 500 1C for 2 h (a) and after MTBE adsorption at 0.5 mbar (b), 5 mbar (c), 10 mbar (d) and 20 mbar (e). ^{1}H MAS NMR spectrum recorded after overnight evacuation of MTBE (previously adsorbed at 20 mbar) at rt (f).

Table 3. H-bond and van der Waals binding energies (kcal/mol) in MTBE-MOR adducts.

	I	II	III
E_H	-10.8	-12.0	-12.9
E_{vdW}	-13.1	-13.9	-15.3

The attribution of the 4.6 ppm peak to silanols interacting with MTBE clusters and/or with single MTBE molecule is confirmed by their intrinsic line width as well as the difference in their intensity ratios at different pressures. The spectral line width for 4.6 ppm peak is narrower and can be due to protons in fast exchange between positions of the nature $(SiOH)_n$-$(MTBE)_n$ and/or $(SiOHAl)_n$-$(MTBE)_n$ via a hoping mechanism. Fig. 5(f) shows a spectrum recorded on a sample (previously adsorbed at 20 mbar) after overnight evacuation of MTBE at rt. It is evident that after such long period of evacuation, MTBE molecules are still strongly adsorbed on MOR (i.e. those strongly stabilized by the side-pockets). Only weakly adsorbed as well as condensed MTBE molecules were removed during evacuation. The spectrum looks

similar to the one recorded at a low pressure of 0.5 mbar (Fig. 5(b)). This means that at low coverage the MTBE molecules are mainly located in the MOR side-pockets.

A weak shoulder at 1.6 ppm appeared in all the spectra (both MTBE adsorbed as well as evacuated samples) and tentatively assigned to t-butyl methyl protons of the MTBE interacting with Brønsted acid sites. Moreover, from the presence of both broad and narrow resonances for MTBE, which are governed primarily by the extent of the molecular environment and/or molecular motion, it is possible to distinguish between different states of MTBE in the adsorbed system. This clearly demonstrates, in full agreement with FTIR results, that MTBE experiences from very weak to strong interactions with the MOR framework in addition to the formation of condensed state at the surface. The evaluation of the ^{13}C MAS NMR data described in the next paragraph will bring more evidence.

In general, NMR is more sensitive to small changes in structure and/or environment than other complementary techniques.[31,32] Standard CPMAS conditions were used to acquire the ^{13}C CPMAS NMR spectra at room temperature with varying cross polarization contact time (CT), in order to discriminate 13C sites based on their mobility. This could divulge different populations of molecules, in particular the rigid ones whose ^{1}H NMR response could have been ignored in the analysis of the ^{1}H spectra due to extensive broadening. Fig. 6 displays C[H] CPMAS NMR spectra acquired on MTBE adsorbed MOR at different pressure. The major signals observed are unambiguously assigned to MTBE, however, the spectra are clearly discrete.

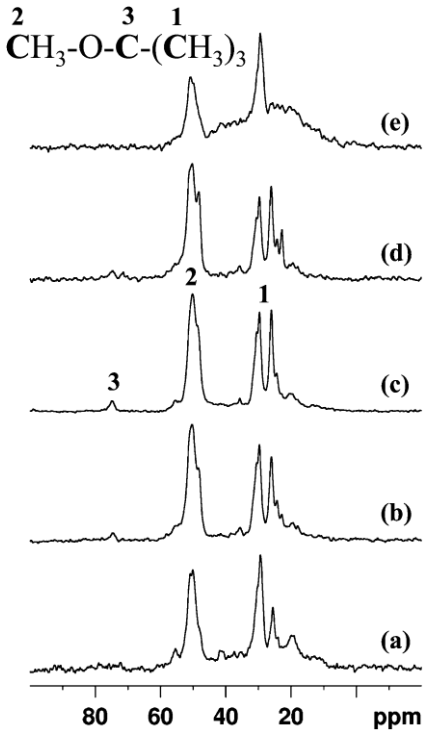

Fig. 6 ^{13}C CPMAS NMR spectra of zeolite MOR after MTBE adsorption at 0.5 mbar (a), 5 mbar (b), 10 mbar (c) and 20 mbar (d). ^{13}C CPMAS NMR spectrum recorded after overnight evacuation of MTBE (previously adsorbed at 20 mbar) at rt (e). A MAS rate of 10 kHz and a CP contact time of 1 ms was used in all the experiments.

At very low adsorption pressure of 0.5 mbar (Fig. 6(a)), resonances due to t-butyl methyl carbons in the range 20–32 ppm and methoxy carbons at 50 ppm as well as tertiary carbon signal at 75 ppm are visible. The line widths for methoxy and tertiary carbons are relatively broad while sharper lines are observed for t-butyl methyl carbons. The appearance of multiple resonances for identical t-butyl methyl carbons (in the range 20–32 ppm) confirms the different environment experienced by the MTBE molecules. At higher pressures (5, 10 and 20 mbar) additional signals from t-butyl methyl carbons in the condensed state appear and dominate with increasing intensity at around 19.6, 22.8, 24.3 and 26 ppm (Fig. 6(b)–(d)). Moreover, the chemical shifts of these narrow signals for t-butyl methyl carbons are closely matched with the shifts observed in the liquid state (spectrum not shown) for MTBE. The new sharp signals appearing for t-butyl methyl carbons and methoxy carbons at 48.5 ppm are attributed to MTBE molecules in a highly mobile state.

Fig. 6, curve e, shows a spectrum recorded after overnight evacuation of MTBE from MOR at rt (previously adsorbed at 20 mbar). It is evident that after such long period of evacuation, only weakly adsorbed as well as condensed MTBE were removed while strongly adsorbed MTBE still remains on MOR side-pockets. Interestingly, Fig. 6 (curve e) shows a very broad component beneath the narrow resonances with a line width several times larger (10–60 ppm range). This anisotropic broadening is consistent with a distribution of rigid environments for the very strongly adsorbed MTBE and thus a reduced mobility of the molecules. This is likely the case for the ether molecules embedded into the restricted space of the MOR side pockets (see for example structure III of Fig. 4). Since the broad component is also visibly present at a very low adsorption pressure of 0.5 mbar (Fig. 6(a)), it can be concluded that the MTBE molecules experience a strong interaction in the MOR side pockets and the adsorbed molecules tend to reach a disordered glassy state.[33] This is also in support to the observation of strongly bound species in ^{1}H MAS NMR and FTIR spectra, where the ether molecules entrapped in the mordenite side pockets were envisaged for their high stability upon evacuation at rt. 13 C line widths are related to the rigidity and/or mobility of spatially confined MTBE molecules which are in turn generated by its site specific interactions with the MOR framework. The ^{13}C CP MAS NMR experiment based on through-space magnetization transfer via ^{1}H–^{13}C hetero-nuclear dipolar coupling favors detection of rigid protonated moieties at short cross polarization CT while mobile protonated moieties at longer CT bring complementary information. At a longer cross polarization contact time of 5 ms (see Fig. SM9 in ESI†) signals observed at short CT are still present at identical chemical shift positions, however, with different intensity ratios. In addition, tertiary carbon signals at 75 ppm are visible in all the spectra.

To summarize, MTBE molecules experience at least three different environments, characterized by their ^{13}C as well as ^{1}H line width and chemical shifts. Firstly, weakly surface bound MTBE, as observed by relatively narrow peaks in the ^{13}C CPMAS NMR at both short and long CT: according to FTIR and computational studies, these species are related to both MTBE H-bonded to the external silanols and to MTBE interacting with the overall zeolite structure by van der Waals forces. Secondly, strongly bound MTBE as observed in the ^{1}H MAS NMR and ^{13}C CPMAS NMR (the very broad peak at CT = 1 ms): MTBE molecules stabilized in the MOR side pockets by both H-bond and van der Waals collective interactions. Finally, mutually interacting MTBE while poorly interacting with framework, if any, observed as a condensed phase.

In addition, MTBE molecules in a non-covalently interacting environment around Brønsted acid sites, although in much lesser concentrations, can’t be ruled out.

C. Analysis of interactions of MTBE adsorbed on different high silica zeolites

The adsorption of MTBE on high silica zeolites (Y, MOR and ZSM-5) is influenced by pore diameter and the topology of the porous network as well as the concentration of the entrapped MTBE molecules, leading to different framework–guest interactions. To define the strength of the interactions occurring between MTBE and different high silica zeolite adsorption sites, spectra collected upon MTBE adsorption at high pressure (30 mbar) and after a subsequent prolonged evacuation were compared in Fig. 7. The spectrum of the bare zeolites outgassed at 500 1C is also reported for comparison.

The spectral features observed upon interaction of MTBE (30 mbar, Fig. 7, curve a^0) on MOR zeolite were described above: beside van der Waals interactions occurring between the ether and zeolite framework at high MTBE doses, interactions with internal silanol species stabilize MTBE molecules inside the porosities of the MOR zeolite. A combination of these forces is responsible for the stability of MTBE in the MOR side pockets, and even after a prolonged evacuation procedure at rt (Fig. 7, curve a^{00}) more than half of the ether molecules are still bound to the zeolite inner surface. This result can be understood if the intensity of the CH_3 stretching bands are compared and microgravimetry data are also taken into account (see next section).

As already commented,[12] when zeolite Y is exposed to 30 mbar MBTE (Fig. 7, curve b^0), the bands of isolated silanol groups at 3745 and 3738 cm^1 almost completely disappeared and, in parallel, two strongly overlapping broad bands at ca. 3380 and 3240 cm^1 are formed. These interactions are associated with the formation of H-bonding of MTBE with internal and external isolated SiOH species, respectively. The bands formed upon adsorption of 30 mbar MTBE on Y zeolite are more intense with respect to MOR zeolite, probably because condensation phenomena largely occur in the mesoporosities of the high silica Y sample. As it can be seen, the evacuation process led to a depletion of bands typical of MTBE interacting with the Y zeolite (Fig. 7,b^{00}), thus indicating that ether is not retained on the zeolite surface.

The IR spectrum of the bare ZSM-5 shows that this solid is characterized by an exceedingly low amount of surface Si–OH species with respect to the other zeolites (Fig. 7,c). In this case, even at high MTBE pressure (Fig. 7,c) only a very low amount of ether is adsorbed, as indicated by the low intensity of bands typical of MTBE molecules, which are mainly adsorbed through van der Waals interactions with the zeolite framework.

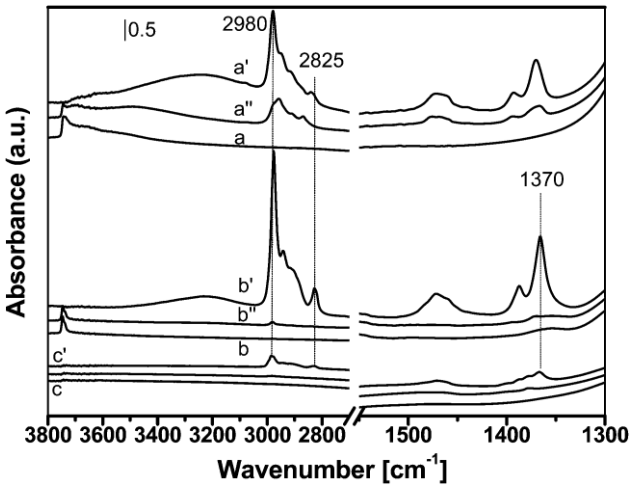

Fig. 7 Infrared spectra of high silica zeolite MOR (a), Y (b) and ZSM-5 (c) outgassed at 500 1C, in contact with 30 mbar (a^0, b^0, c^0) of MTBE and subsequent evacuation for 40^0 (a^{00}, b^{00}, c^{00}), respectively.

Finally, in order to evaluate the adsorption capacity of the different zeolites, gravimetric measurements were performed at 35 °C on the samples pretreated in vacuum at the same temperature (Fig. 8). The experiment on MOR zeolite was performed by outgassing the sample at 100 1C: as determined by TGA and FTIR, this temperature is needed to completely remove adsorbed water from the zeolite surface.

The isotherm of MOR zeolite (Fig. 8A) shows three different adsorption regimes. From the analysis of the curve (both in adsorption and desorption branches) it can be observed that at pressure lower than 0.8 mbar, the MTBE uptake as a function of equilibrium pressure is quite steep thus indicating the high affinity of MTBE for the MOR surface. Then, the curve slope decreases up to 3 mbar, when it gradually comes to a plateau. These trends testify the different strength of interactions that are present between MTBE and MOR adsorbent in the three different regimes. Between 0 and 0.8 mbar the MTBE uptake determined using the desorption branch is of 7.8% zeolite dry weight (DW), and becomes 9% and 10.6% zeolite DW at 3 and 30 mbar, respectively. In agreement with FTIR, the first adsorption region is associated with the interaction of MTBE with surface silanol species (mainly in internal position of MOR cages), the second step is mainly related to adsorption of MTBE on external silanols and, finally, the third region is consistent with the condensation of MTBE molecules inside MOR cages and on the external surface of the zeolite crystals. Very interestingly the desorption branch of the isotherm is not completed, as a consistent fraction (ca. 6.1 wt%, corresponding to ca. 2 MTBE per u.c.) of MTBE is still bound to the MOR side-pockets, in agreement with FTIR results.

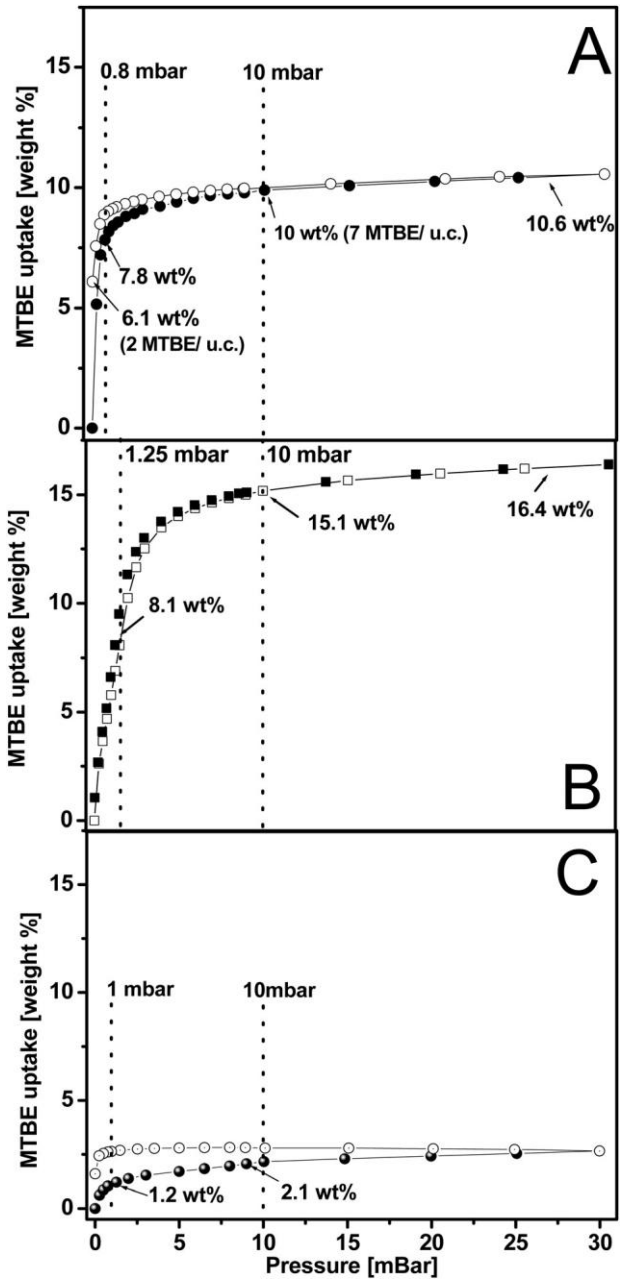

Fig. 8 MTBE gravimetric adsorption (full circles) and desorption (empty circles) isotherms measured at 35 1C on high-silica zeolite MOR (A), Y (B) and ZSM5 (C).

Concerning zeolite Y (Fig. 8B), three different regimes can also be determined by the analysis of the curves, both in adsorption and in desorption branches, which are almost coincident. At low and medium pressure regimes the MTBE uptake shows a curve slope lower than that of the MOR. Between 0 and 1.25 mbar, MTBE uptake determined using the desorption branch is of 8.1% zeolite dry weight (DW), whereas

between 1.25 and 10 mbar, the uptake is of 7.0% zeolite DW. From this pressure upward, the MTBE overall uptake is equal to 16.4% zeolite DW. Gravimetric analysis, in agreement with IR results (vide supra), indicates that the amount of adsorbed MTBE is much higher in Y absorbent than in MOR zeolite. Nevertheless, it has to be taken into account that the surface area of Y zeolite is twice with respect to the MOR solid. At low pressures, for both Y and MOR, MTBE molecules interact with silanol groups, forming silanol–MTBE H-bonded complexes. Nevertheless, the slope of the isotherms suggest that the affinity of MTBE for MOR solid is higher than in Y zeolite. At pressures higher than ca. 1 mbar, the adsorption is likely driven by van der Waals interactions between zeolite walls and MTBE molecules (host–guest) and between MTBE molecules (guest–guest), which further cause condensation at pressures higher than 10 mbar.

ZSM-5 has a different adsorption behavior in comparison with the Y and MOR zeolites. In fact, the ZSM-5 isotherm shows a slope change at 0.5 mbar. At pressures lower than 0.5 mbar, the MTBE uptake is low (ca. 1% zeolite DW), then the curve slope decreases up to 7 mbar (ca. 1.8% zeolite DW), when it gradually comes to a plateau. Between 0 and 0.5 mbar, MTBE uptake determined using the desorption branch is of 1% zeolite DW; between 0.5 and 7 mbar, the uptake is of 0.8% zeolite DW. From this pressure upward, the MTBE overall uptake remains of ca. 2.7% zeolite DW. For zeolite ZSM-5, the interaction between silanol groups and MTBE molecules is negligible since the amount of silanols is very low, thus the adsorption is due to van der Waals interactions already at low pressures.

The observation of hysteresis loops in the case of isotherms of MTBE adsorbed on both ZSM-5 and MOR zeolites deserves some additional comments. Indeed, this phenomena can be associated with diffusion effects within the micropores present in both zeolites. The phenomenon is, in fact, more evident for ZSM-5 than for the MOR zeolite, whereas it is not observed for the Y zeolite. Interestingly, this last solid presents two families of micropores with diameter of 13 and 22 Å, (the total volume of micropores being 0.32 cm^3 g^1), whereas MOR zeolite is characterised by three families of micropores of 9, 11 and 14 Å with a total volume of 0.20 cm^3 g^1. Finally, ZSM-5 contains the smallest micropores of ca. 8 Å, with a volume of 0.16 cm^3 g^1.

Conclusions

The effect of surface and textural properties of high-silica zeolites, ZSM-5, mordenite (MOR) and Y zeolites, on MTBE adsorption was investigated by means of experimental and computational approaches.

As derived by N_2 physisorption, besides the zeolite micropores, structural mesoporosity in Y and large micropores in MOR (i.e. formed by fusing together two adjacent side-pockets) zeolites are formed as a consequence of dealumination processes.

FTIR analysis on zeolites outgassed at both room temperature (or 100 1C for MOR) and 500 1C allowed definition of the relative distribution of surface OH sites of the different samples: the dealuminated MOR zeolite is highly defective, its surface being populated by isolated SiOH species located on both external and internal zeolite surfaces and SiOH species interacting each other via H-bonding interactions. Experimental IR studies of surface SiOH species were also augmented by computational studied that allowed to model a variety of silanol species in MOR side pockets.

Interacting SiOH are also present in Y zeolite but in lower concentration with respect to MOR. The thermogravimetric analysis shows that the overall concentration of point defects (i.e. silanol groups) of these solids is ca. 0.56 and 3.71 OH per nm^2 for Y and MOR zeolites, respectively. By contrast, the ZSM-5 zeolite is characterized by a negligible amount of SiOH groups.

The contribution of the different surface groups of MOR to the MTBE adsorption was clarified by outgassing the zeolite at 500 1C. The treatment led to a strong reduction of silanol species interacting each other through H-bonding and to a better definition of stretching vibration of isolated silanols in both external and internal zeolite surfaces. FTIR and SS-NMR of adsorbed MTBE allowed monitoring different types of interactions (both H-bonding and van der Waals) and several complexes formed between ether molecules and MOR surface.

At low MTBE dosage (below 0.8 mbar), the downward shifts of stretching modes for isolated silanols in internal position (originally vibrating at 3735 cm^1) of MOR cavities and with species weakly interacting each other through H-bonding (vibrating at 3650 cm^1) are consistent with medium–weak H-bonding with the MTBE oxygen atom, the associated Dn_{OH} shift being around 300–400 cm^1. These shifts are lower than those related to the interaction occurring with external silanols (Dn_{OH} = 500 cm^1). The persistency of irreversibly adsorbed MTBE showed that confinement effects governed by dispersive (van der Waals) forces play an important role in stabilizing the ether molecules inside the zeolite cages. As clearly stated by DFT studies, H-bond and van der Waals energies of comparable entity are involved in MTBE–silanol complexes formed inside the mordenite side-pockets. At a higher MTBE dosage, no silanol groups remain available and the adsorption occurs at the siloxane network of the zeolite via dispersive forces.

In full agreement with FTIR and DFT calculations, SS-NMR shows that at the maximum zeolite coverage (20 mbar, ca. 11 wt%) MTBE molecules experience at least three different environments, characterized by specific ^{13}C and ^{1}H line width and chemical shifts: (i) weakly bound MTBE, as observed by relatively narrow peaks in the ^{13}C CPMAS NMR; (ii) strongly bound MTBE as observed in the ^{1}H MAS NMR and ^{13}C CPMAS NMR (a very broad peak at short contact time of 1 ms); (iii) mutually interacting MTBE observed as a condensed phase (narrow ^{1}H and ^{13}C line widths closely matching with the chemical shifts of liquid MTBE).

Finally, FTIR analysis was also used to study the MTBE adsorption on Y and ZSM-5 zeolites. As observed for MOR zeolite, because of the cage confinement effects, the MTBE molecules interact more strongly when embedded in the internal cavities of the Y zeolite than on the external surfaces, though the latter provide stronger H-bonds with the ether molecule. At high MTBE loading, van der Waals interactions with siloxane species of Y zeolite are responsible for the adsorption process. These interactions are those mainly driving the adsorption of MTBE on ZSM-5 zeolite, which is characterized by a negligible amount of SiOH species. Gravimetric analysis also confirmed the sorption capacities of the three zeolites and their highly different affinity to MTBE molecules.

Acknowledgements

Research co-funded by Research Center for Non-Conventional Energy, Istituto ENI Donegani – Environmental Technologies (Novara, Italy). The authors thank Dr. Claudio Cassino for liquid state NMR measurements.

References

1 H. W. Hung and T. F. Lin, J. Hazard. Mater., 2006, 135, 210–217.

2 OEHHA (Office of Environmental Health Hazard Assessment), Public Health Goal for Methyl Tertiary Butyl Ether (MTBE) in Drinking Water, Pesticide and Environmental Toxicology Section, California EPA, USA, 1999. 3 P. J. Squillace, J. S. Zogorski, W. G. Wilber and C. V. Price, Environ. Sci. Technol., 1996, 30, 1721–1730. 4 B. N. Chisala, N. G. Tait and D. N. Lerner, J. Contam. Hydrol., 2007, 91, 128–145.

5 W. T. Tzsai, K. J. Hsien and H. C. Hsu, J. Hazard. Mater., 2009, 166, 635–641.

6 Q. Hao, X. R. Xu, S. Li, J. L. Liu, Y. Y. Yu and H. B. Li, Int. J. Environ. Bioenergy, 2012, 1(2), 93–104. 7 A. Rossner and D. R. U. Knappe, Water Res., 2008, 42, 2287–2299.

8 S. Li, V. A. Tuan, R. D. Noble and J. L. Falconer, Environ. Sci. Technol., 2003, 37, 4007–4010.

9 M. A. Anderson, Environ. Sci. Technol., 2000, 34, 725–727. 10 R. Arletti, A. Martucci, A. Alberti, L. Pasti, M. Nassi and R. Bagatin, J. Solid State Chem., 2012, 194, 135–142.

11 M. G. Ahunbay, O. Karvan and A. Erdem-Senatalar, Microporous Mesoporous Mater., 2008, 115, 93–97.

12 I. Braschi, G. Gatti, C. Bisio, G. Berlier, V. Sacchetto, M. Cossi and L. Marchese, J. Phys. Chem. C, 2012, 116, 6943–6952.

13 (a) R. Ahlrichs, M. Bar, M. Haser, H. Horn and C. Kolmen, Chem. Phys. Lett., 1989, 162, 165–169; (b) M. Arnim and R. J. Ahlrichs, Chem. Phys., 1999, 111, 9183–9190.

14 (a) A. D. Becke, Phys. Rev. A: At., Mol., Opt. Phys., 1988, 38, 3098–310; (b) C. Lee, W. Yang and R. G. Parr, Phys. Rev. B, 1988, 37, 785–789.

15 A. D. Becke, J. Chem. Phys., 1993, 98, 1372–1377.

16 (a) P. C. Hariharan and J. A. Pople, Theor. Chim. Acta, 1973, 28, 213–222; (b) T. H. Dunning, J. Chem. Phys., 1989, 90, 1007–1023.

17 P. J. Hay and W. R. Wadt, J. Chem. Phys., 1985, 82, 299–310.

18 S. J. Grimme, J. Comput. Chem., 2006, 27, 1787–1799.

19 R. Szostak, Stud. Surf. Sci. Catal., 2001, 137, 261.

20 J. Cejka, Zeolites and Ordered Mesoporous Materials: Progress and Prospects, The 1st FEZA School on Zeolites, Prague, Czech Republic, 1st edn, August 20–21, 2005, vol. 157.

21 I. Braschi, G. Gatti, G. Paul, C. E. Gessa, M. Cossi and L. Marchese, Langmuir, 2010, 26, 9524–9532. 22 I. Braschi, S. Blasioli, L. Gigli, C. E. Gessa, A. Alberti and A. Martucci, J. Hazard. Mater., 2010, 178, 218–225.

23 T. Kawai and K. Tsutsumi, Adsorption, 1998, 4, 225–231.

24 H. H. Baik and D. Barthomeuf, J. Chem. Soc., Faraday Trans. 1, 1979, 75, 2366–2376.

25 R. W. Olsson and L. D. Rollmann, Inorg. Chem., 1977, 16, 651–654.

26 A. Martucci, M. A. Cremonini, S. Blasioli, L. Gigli, G. Gatti, L. Marchese and I. Braschi, Microporous Mesoporous Mater., 2013, 170, 274–286.

27 I. Braschi, G. Paul, G. Gatti, M. Cossi and L. Marchese, RSC Adv., 2013, 3, 7427–7437.

28 S. Ban, A. N. C. van Laak, J. Landers, A. V. Neimark, P. E. de Jongh, K. P. de Jong and T. J. H. Vlugt, J. Phys. Chem. C, 2010, 114, 2056–2065.

29 M. Muller, G. Harvey and R. Prins, Microporous Mesoporous Mater., 2000, 34, 135–147.

30 M. Hunger, S. Ernst, S. Steuernagel and J. Weitkamp, Microporous Mater., 1996, 6, 349–353.

31 N. Baccile and F. Babonneau, Microporous Mesoporous Mater., 2008, 110, 534–542.

32 T. Azais, C. T. Peteilh, F. Aussenac, N. Baccile, C. Coelho, J.-M. Devoisselle and F. Babonneau, Chem. Mater., 2006, 18, 6382–6390.

33 T. Horvath, M. Seiler and M. Hunger, Appl. Catal., A, 2000, 193, 227–236.